

Resolution-independent modeling of environmental effects in semi-analytic models of galaxy formation that include ram-pressure stripping of both hot and cold gas

Yu Luo^{1,2,4} ^{*}, Xi Kang¹, Guinevere Kauffmann², Jian Fu³

¹*Purple Mountain Observatory, the Partner Group of MPI für Astronomie, 2 West Beijing Road, Nanjing 210008, China*

²*Max-Planck Institut für Astrophysik, 85741 Garching, Germany*

³*Key Laboratory for Research in Galaxy and Cosmology, Shanghai Astronomical Observatory, Chinese Academy of Science, 80 Nandan Road, Shanghai 200030, China*

⁴*Graduate School, University of the Chinese Academy of Science, 19A, Yuquan Road, Beijing 100049, China*

10 August 2018

ABSTRACT

The quenching of star formation in satellite galaxies is observed over a wide range of dark matter halo masses and galaxy environments. In the recent Guo et al (2011) and Fu et al (2013) semi-analytic + N-body models, the gaseous environment of the satellite galaxy is governed by the properties of the dark matter subhalo in which it resides. This quantity depends of the resolution of the N-body simulation, leading to a divergent fraction of quenched satellites in high- and low-resolution simulations. Here, we incorporate an analytic model to trace the subhaloes below the resolution limit. We demonstrate that we then obtain better converged results between the Millennium I and II simulations, especially for the satellites in the massive haloes ($\log M_{\text{halo}} = [14, 15]$). We also include a new physical model for the ram-pressure stripping of cold gas in satellite galaxies. However, we find very clear discrepancies with observed trends in quenched satellite galaxy fractions as a function of stellar mass at fixed halo mass. At fixed halo mass, the quenched fraction of satellites does not depend on stellar mass in the models, but increases strongly with mass in the data. In addition to the over-prediction of low-mass passive satellites, the models also predict too few quenched *central* galaxies with low stellar masses, so the problems in reproducing quenched fractions are not purely of environmental origin. Further improvements to the treatment of the gas-physical processes regulating the star formation histories of galaxies are clearly necessary to resolve these problems.

Key words: galaxies: evolution - galaxies: formation - stars: formation - galaxies: ISM

1 INTRODUCTION

Many of the observed properties of galaxies, such as their colors, morphologies, star formation rates (SFR) and gas-to-star fractions, are observed to have strong dependence on their environment (e.g. Kauffmann et al. 2004; Bamford et al. 2009; Boselli et al. 2014). Galaxies in clusters or groups tend to have redder colors, bulge-dominated morphologies, lower gas-to-star ratios and less star formation than isolated galaxies of similar mass (Butcher & Oemler 1978; Dressler 1980; Balogh et al. 2004; Baldry et al. 2006). This dependence is believed to arise from the interplay between the

gas component of galaxies and their environment; unlike the stellar component, the gas can be easily affected by the ambient pressure in galaxy groups or clusters.

When a galaxy moves through a cluster, the ram pressure (hereafter RP, Gunn & Gott 1972) of the intra-cluster medium (ICM) acts to strip both the hot gas reservoir and the cold interstellar gas, and this process plays an important role in the star formation history in the galaxy. Many studies have concluded that this stripping process is the main cause for the increase of S0 galaxies in rich clusters (e.g. Biermann & Tinsley 1975; Dressler 1980; Whitmore, Gilmore & Jones 1993). In the last decade, observations have revealed direct evidence for ram-pressure stripping of gas in cluster galaxies in the form of long gaseous tails trailing behind these sys-

* E-mail: luoyu, kangxi@pmo.ac.cn

tems (e.g. Kenney et al. 2004; Crowl et al. 2005; Sakelliou et al. 2005; Machacek et al. 2006). The same process is also invoked as an explanation of the depletion of the cold gas in galaxies in clusters (Boselli & Gavazzi 2006), often referred to as “HI deficiency” (e.g. Haynes & Giovanelli 1984; Solanes et al. 2001; Hughes & Cortese 2009).

To understand the effects of RP stripping on the galaxy gas component in detail, numerical hydrodynamical simulations are the ideal tools. Abadi et al. (1999) presented the first study of RP stripping using an idealized SPH simulation, followed by more realistic hydrodynamical simulations (e.g., Roediger & Hensler 2005; Roediger & Brüggem 2007; McCarthy et al. 2008; Tonnesen & Bryan 2009, Tecce et al. 2010). These studies showed that RP can strip a significant amount of hot gas and cold gas from galaxies and can quickly reduce the total SFR (e.g., Tonnesen & Bryan 2012). However, it has also been argued (Bekki 2014) that star formation can also be enhanced by RP, and that the reduction/enhancement will depend on model parameters such as halo mass, peri-centric distance with respect to the centre of the cluster etc.

In semi-analytic models (SAMs) of galaxy formation, the descriptions of the effect of RP on the gas component are very simplistic. In early versions, satellite galaxies were assumed to lose their hot gaseous haloes immediately after falling into a bigger halo (e.g., Kauffmann et al. 1993; Somerville et al. 1999; Cole et al. 2000; Kang et al. 2005; Bower et al. 2006; De Lucia & Blaizot 2007 (hereafter DLB07)). It was then found (e.g., Kang & van den Bosch 2008; Kimm et al. 2009) that the instantaneous stripping of the hot gas causes the over-prediction of red satellite galaxies in the clusters. In later models (e.g., Kang & van den Bosch 2008; Font et al. 2008; Weinmann et al. 2010; Guo et al. 2011, hereafter Guo11)), the stripping of hot gas is treated in a more continuous way, i.e. the mass loss rate of hot gas halo is assumed to be the same as that of dark matter subhalo in which the satellite resides. Including only the stripping of hot halo gas is not physically plausible; the stripping of cold gas in galaxies is also needed to account for the observed cold gas depletion in satellites (Fabello et al. 2012; Li et al. 2012b; Zhang et al. 2013). Stripping of cold gas has been included in some models (Okamoto & Nagashima 2003; Lanzoni et al. 2005), and has been found to have negligible effect on the colors and SFRs of satellite galaxies.

Because the stripping of gas in the satellite depends on the competition between the RP from the hot gas and the gravitation of the satellite itself, it is important to model the local environment of satellite galaxies accurately. In N-body simulations, the local environment at the subhalo level will be dependent on the resolution of the simulation. In low-resolution simulation, the evolution of subhalo can not be traced to very low mass due to the number threshold used to identify subhalo, and for given mass a subhalo in low-resolution simulation contains less number of particles, making its identification more difficult. In the central region of halo the identification of subhalo is more challenging as the background density is high (Onions et al. 2012). We also note that the physical descriptions of processes such as gas cooling, feedback, stripping etc, are very often tied to the properties of the subhalo (Springel et al. 2001; Kang et al. 2005; Bower et al. 2006; Guo et al. 2011;), and these descriptions will then also be dependent on resolution. This

will lead to non-convergent results between different resolution simulations, as found in recent studies (Fu et al. 2013; Lagos et al. 2014; Guo & White 2014), and it also raises the concern that the high fraction of passive galaxies in low-resolution simulation is a consequence of resolution effects.

In this paper, we study the quenched fraction of galaxies in different environments with and without the effects of RP stripping. We adopt the version of L-Galaxies model described in Fu et al. (2013, hereafter Fu13), which is a recent version of the Munich semi-analytic model that includes the radial distribution of molecular and atomic gas in galaxy disks. This model allows us to model the cold gas stripping as a function of radius in the galaxy. We improve the Fu13 model by 1) using a consistent description of physics for satellites whose subhaloes cannot be resolved. Our resolution-independent prescriptions can also be applied to other SAMs based on merger trees from N-body simulations. 2) We add a model for the effect of RP stripping on the cold gas in galactic disks. These improvements allow us to model ram pressure stripping of cold gas at different radii in disks, and to study how the environment can affect the HI, H₂, and star formation.

This paper is organized as follows. In Section 2, we first briefly summarize the L-Galaxies model and then describe the changes we make to Fu13 model. In Section 3, we analyze stellar/gas mass functions and galaxy clustering, and we compare our model results with recent observations of the properties of satellite galaxies, such as their specific star formation rates and gas fractions. We test the degree to which our new models give convergent results between two N-body simulations of different resolution, and we analyze the effect of RP stripping in cluster environments. In Section 4, we summarize our results and discuss possibilities for future work.

2 THE MODEL

In this section, we briefly introduce the N-body simulations used in this work as well as the L-Galaxies models, and then describe in detail the main changes to the physics made with respect to the previous models.

2.1 N-body simulations and L-Galaxies model

Our work in this paper is based on the Munich semi-analytic galaxy formation model, L-Galaxies, which has been developed over more than two decades (e.g., White & Frenk 1991; Kauffmann et al. 1993; Kauffmann et al. 1999; Springel et al. 2001; Croton et al. 2006; De Lucia & Blaizot 2007; Guo et al. 2011&2013; Fu et al. 2010 & 2013; Henriques et al. 2015). The L-Galaxies model has been implemented on two main N-body cosmological simulations: The Millennium Simulation (hereafter MS, Springel et al. 2005) and Millennium-II simulation (hereafter MS-II, Boylan-Kolchin et al. 2009). The two simulations have the same number of particles and cosmology parameters, but the MS-II has 1/125 the volume of MS, but 125 times higher in mass resolution. Angulo & White (2010) developed a method to rescale the cosmological parameters from the WMAP1 to the WMAP7 cosmology. For MS, the box size is rescaled from 500 Mpc h⁻¹ to 521.555 Mpc h⁻¹, and the particle

mass is changed from $8.6 \times 10^8 M_\odot h^{-1}$ to $1.06 \times 10^9 M_\odot h^{-1}$; for MS-II, the box size is rescaled to $104.311 \text{ Mpc } h^{-1}$, and $8.50 \times 10^6 M_\odot h^{-1}$ for the particle mass. In this paper, we follow Angulo & White (2010) and use the runs appropriate for the WMAP7 cosmology, with parameters as follows: $\Omega_\Lambda = 0.728$, $\Omega_m = 0.272$, $\Omega_{\text{baryon}} = 0.045$, $\sigma_8 = 0.807$ and $h = 0.704$.

In SAMs, galaxies are assumed to form at the centres of the dark matter haloes. The evolution of the haloes is followed using merger trees from the N-body cosmological simulations, and the models describe the physical processes relevant to the baryonic matter, e.g re-ionization, hot gas cooling and cold gas infall, star formation and metal production, SN feedback, hot gas stripping and tidal disruption in satellites, galaxy mergers, bulge formation, black hole growth, and AGN feedback. The detailed descriptions of these physical processes can be found in Section 3 of Guo11.

In the L-Galaxies model, galaxies are classified into three types. Type 0 galaxies are those located at the centre of the main haloes found with a Friends-of-Friends (FOF) algorithm in the simulation outputs. A Type 0 galaxy is a ‘‘central’’ galaxy with its own hot gaseous halo, and the hot gas distributes isothermally in the dark matter halo. The hot gas can cool onto the central galaxy disk through a ‘‘cooling flow’’ or a ‘‘cold flow’’, and the cold gas is the source of star formation. An instantaneous recycling approximation is adopted for mass return from evolved stars and for the injection of metals into the ISM; this implies that the massive stars explode as SN at the time when they form.¹ The SN feedback energy reheats part of disk cold gas into the hot gaseous halo of the central galaxy. If the SN energy is large enough, part of the hot gaseous halo can be ejected out of the dark matter potential and become ejected gas. With the growth of the dark matter halo, the ejected gas will be reincorporated back to the central halo.

Both Type 1 and Type 2 galaxies are regarded as satellite galaxies in the model. A Type 1 galaxy is located at the center of a subhalo, which is an overdensity within the FoF halo (Springel et al. 2001). The haloes/subhaloes contain at least 20 bound particles for both MS and MS-II (Springel et al. 2005, Boylan-Kolchin et al. 2009). Boylan-Kolchin et al. (2009) have pointed that above this particle number (20) the abundance of subhaloes between two simulations differs only about 30%, and with more than 50-100 particles the results agree much better. Type 1 galaxies have their own hot gaseous haloes, so gas can cool onto these galaxies. Cold gas reheated by the SN explosions in a Type 1 will be added to the hot gaseous halo of its own subhalo or the halo of the central Type 0 galaxy, depending on the distance between the Type 1 and the central object. A Type 2 galaxy is an ‘‘orphan galaxy’’, which no longer has an associated dark matter subhalo. A Type 2 galaxy does not have a hot gaseous halo and thus has no gas cooling and infall. The supernova reheated cold gas from Type 2 is added to its central galaxy, i.e., the associated Type 0 or Type 1 object.

Both Type 1 and Type 2 galaxies are initially born as Type 0 objects. They become Type 1 when they fall into a group or cluster and may later become type 2 after their

dark matter subhaloes are disrupted by tidal effects or the subhaloes are not well resolved in the low-resolution simulation. Type 1 and 2 galaxies may later merge into the central galaxy of their host (sub)halo. In Guo11 & Fu13, the hot gaseous halo and ‘‘ejected reservoir’’ of a Type 1 galaxy can be stripped by RP when the force of RP dominates over its self-gravity. A Type 2 galaxy can be disrupted entirely by tidal forces exerted by the central object, if the density of the main halo through which the satellite travels at pericentre is larger than the average baryonic mass density of the Type 2.

In this paper, we update the semi-analytic models of Fu et al. (2013), which is a branch of the recent L-Galaxies model. Compared with the previous L-Galaxies models, Fu13 contains the following two main improvements:

- (i) Each galaxy disk is divided into multiple rings, and thus the evolution of the radial distribution of cold gas and stars can be traced.
- (ii) A prescription for the conversion of atomic gas into molecular gas is included, and the star formation is assumed to be directly proportional to the local surface density of molecular gas $\Sigma_{\text{SFR}} \propto \Sigma_{\text{H}_2}$.

These improvements enable us to calculate whether the RP at a certain radius in the galaxy disk is sufficient to remove the gas, and thus to trace the depletion of atomic and molecular gas in cluster galaxies.

In this paper, We make two further main changes to the Fu13 model:

- (1) we introduce an analytic method to trace the mass evolution of unresolved subhaloes once they are not resolved by the simulation. This enables us to model the evolution of low-mass satellite galaxies in a resolution-independent way.
- (2) we include new prescriptions for ram pressure stripping of the cold gas;

In the following sections, we describe our modifications in detail.

2.2 Tracing galaxies in unresolved subhaloes

As discussed in Section 1, the properties of low-mass satellite galaxies predicted by L-galaxies will be resolution dependent, because the treatment of the physics depends on whether or not the subhalo of the satellite is resolved by the simulation (i.e. whether the galaxy is Type 1 or Type 2). The detailed issues are the following:

(i) For satellite galaxies, $M_{\text{vir}}, V_{\text{vir}}, R_{\text{vir}}$ and V_{max} are fixed at the moment they first fall into a larger halo, whereas M_{sub} is measured in each simulation output until the subhaloes are disrupted. M_{sub} for a Type 2 will be fixed at the last time when it was a Type 1, which will be strongly dependent on the resolution of the simulation.

(ii) The hot gas in a subhalo is assumed to be distributed the same way as the dark matter. When a subhalo is disrupted and the galaxy becomes a Type 2, it is assumed to lose its hot gas and ejected gas reservoirs immediately. Thus, gas cooling, infall and reincorporation no longer take place if the galaxy is a Type 2.

(iii) Only Type 2 galaxies can be disrupted by the tidal force of central galaxies.

These three assumptions will cause inconsistencies between models based on dark matter simulations with different res-

¹ Yates et al. 2014 considered more realistic model for chemical enrichment of different elements.

olutions, because many Type 1 galaxies in a high resolution simulation will be Type 2 galaxies in low resolution simulations (e.g. Fig.A1 in Guo11).

In the following section, we incorporate the model of Jiang & van den Bosch (2014, hereafter JB14) to trace the evolution of a subhalo after it is no longer resolved by the N-body simulation. In this way we can estimate the key properties of unresolved subhaloes, such as M_{sub} , V_{max} , and treat Type 2s in the same way as Type 1s. We will then show that this procedure helps to alleviate the resolution-dependent properties of satellite galaxies in the models.

2.2.1 An analytic model for subhalo evolution

According to JB14, the average mass loss rate of a subhalo depends only on the instantaneous mass ratio of the subhalo mass m and parent halo M ,

$$\dot{m} = -\varphi \frac{m}{\tau_{\text{dyn}}} \left(\frac{m}{M}\right)^{\zeta} \quad (1)$$

where φ and ζ are free parameters, τ_{dyn} is the halo's dynamical time

$$\tau_{\text{dyn}}(z) = \sqrt{\frac{3\pi}{16G\rho_{\text{crit}}(z)}}, \quad (2)$$

where $\rho_{\text{crit}}(z)$ is the critical density at redshift z . So we can get the subhalo mass $m(t + \Delta t)$ in a static parent halo at $t + \Delta t$ as:

$$m(t + \Delta t) = m(t) \left[1 + \zeta \left(\frac{m}{M}\right)^{\zeta} \left(\frac{\Delta t}{\tau}\right)\right]^{-1/\zeta} \quad (3)$$

where $\tau = \tau(z)/\varphi$ is the characteristic mass loss time scale at redshift z . We adjust the parameters ζ and φ so that the distribution of the predicted distribution of M_{sub} for all Type 1 galaxies at $z = 0$ matches the distribution of M_{sub} for Type 1 galaxies measured directly from the $z = 0$ simulation output. The best-fit values we find are $\zeta = 0.07$, $\varphi = 9.5$. Note that our φ is much larger than the value of JB14 (their best value is 1.34) and the difference is mainly due to the definition of ρ . If we use the same definition as JB14, our best fitted φ is about 40% lower than that of JB14.

JB14 also provides a formula to estimate the V_{max} of subhalo during the evolution. They find that V_{max} evolves more slowly than the mass evolution, because V_{max} is mainly determined by the inner region of the subhalo which is not strongly affected by the tidal force of the host halo. For simplicity and consistency with Guo11, we keep the V_{max} for the Type 2 satellite also fixed at the value when it was last a Type 0 object. This means that the main change with respect to the Guo11 model occurs after the subhaloes have been fully tidally disrupted. So we only apply the above model for subhalo mass evolution after it is not resolved in the simulation.

2.2.2 A consistent treatment of the physics of satellite galaxies

In the Guo11 and Fu13 models, Type 2s lose all their hot gas after their subhaloes are disrupted. Using the methodology outlined in Sec.2.2.1, we can now estimate the evolution of subhaloes to arbitrarily low masses, and thus Type 2 galaxies will retain their own hot gas haloes and lose hot gas

continuously through stripping processes in the same way as Type 1s. The hot gas is assumed to have a isothermal distribution:

$$\rho_{\text{hot}}(r) = \frac{M_{\text{hot}}}{4\pi R_{\text{vir}} r^2} \quad (4)$$

When Type 2s fall within the virial radius of the central galaxy, we calculate the stripping radius as $R_{\text{strip}} = \min(R_{\text{tidal}}, R_{\text{r.p.}})$. We use Eq. 25 and 26 in Guo et al. (2011) to calculate R_{tidal} and $R_{\text{r.p.}}$:

$$R_{\text{tidal}} = \left(\frac{M_{\text{sub}}}{M_{\text{sub, infall}}}\right) R_{\text{vir, infall}} \quad (5)$$

where M_{sub} is the subhalo mass given by Eq.1, $M_{\text{sub, infall}}$ and $R_{\text{sub, infall}}$ are the dark matter mass and virial radius of the subhalo at the last time when it was Type 0.

$$\rho_{\text{sat}}(R_{\text{r.p.}}) V_{\text{sat}}^2 = \rho_{\text{par}}(R) V_{\text{orbit}}^2 \quad (6)$$

where $\rho_{\text{sat}}(R_{\text{r.p.}})$ is the hot gas density of the satellite at $R_{\text{r.p.}}$; V_{sat} is the virial velocity of the subhalo; $\rho_{\text{par}}(R)$ is the hot gas density of the main halo at the distance R ; and V_{orbit} is the orbital velocity of the satellite (we simply use the virial velocity of the main halo).

All the hot gas beyond R_{strip} is removed and added to the hot gas component of the parent central galaxy. Then we set the hot gas radius to be $r_{\text{hot}} = R_{\text{strip}}$. The hot gas in Type 2s will cool and fall onto the galaxy disk with an exponential surface density distribution

$$\Sigma_{\text{gas}}(r) = \Sigma_{\text{gas}}^{(0)} \exp(-r/r_{\text{infall}}) \quad (7)$$

where the infall scale length $r_{\text{infall}} = (\lambda/\sqrt{2})r_{\text{vir}}$. We keep the original spin parameter λ and r_{vir} when the galaxy was last a Type 0 unchanged.

In the models of Guo11 and Fu13, SN feedback reheats the cold gas in the disk, and if there is remaining energy, hot gas will be ejected out of the halo. In the Guo11 code, the supernova reheating efficiency ϵ_{disk} is written as

$$\epsilon_{\text{disk}} = \epsilon \times \left[0.5 + \left(\frac{V_{\text{max}}}{V_{\text{reheat}}}\right)^{-\beta_1}\right] \quad (8)$$

The supernova ejection efficiency is written as

$$\epsilon_{\text{halo}} = \eta \times \left[0.5 + \left(\frac{V_{\text{max}}}{V_{\text{eject}}}\right)^{-\beta_2}\right], \quad (9)$$

The efficiency of the SN feedback in Type 2s is assumed to scale with the maximum circular velocity V_{max} of its central galaxy and reheated gas from Type 2s is added to the hot gas component of the central galaxy. We note that in Guo11, Type 2s have no hot gas component. Here, we assume SN in Type 2s will reheat cold gas to its own hot gas component and allow for an ejected gas reservoir in Type 2s in the same way as for Type 0s and 1s. Due to the fact that hot gas is stripped from satellites, only a fraction $R_{\text{hot}}/R_{\text{vir}}$ of reheated gas remains in the subhalo and the rest is returned to the main halo. We replace V_{max} of the Type 2s' central galaxy with the V_{max} for the Type 2 galaxy is taken as the value of V_{max} when it was last a Type 0. Note that in our new model, the SN heating efficiency in a Type 2 is determined by its own V_{max} , which has a lower value than the V_{max} of the central galaxy that is used to scale the SN reheating efficiency in a satellite galaxy in the Guo11 and Fu13 models. This choice is also motivated by some recent work (e.g., Lagos

et al. 2013; Kang 2014) which shows that SN feedback is more likely determined by the local galaxy potential. Usually the V_{\max} of satellite is lower than V_{\max} of the central, so the SN heating efficiency is higher in satellite galaxies in our model and we will later show in Section 3.2 that it leads to a slightly better agreement with the observed galaxy two-point correlation function on small scales in low stellar mass bins.

The hot gas in the subhaloes of Type 2s will cool and fall onto the gas disks of Type 2s later on. With the growth of the dark matter halo, the ejected gas in the subhalo will be reincorporated into the hot gas again. The reincorporation efficiency is

$$\dot{M}_{\text{ejec}} = -\gamma \left(\frac{V_{\text{vir}}}{220} \right) \left(\frac{M_{\text{ejec}}}{t_{\text{dyn,h}}} \right), \quad (10)$$

where γ is free parameter, $t_{\text{dyn,h}} = R_{\text{vir}}/V_{\text{vir}}$ is the halo dynamical time.

Finally, we note that in the Guo11 model, only Type 2 galaxies are disrupted by tidal forces (see Sec. 3.6.2 in Guo11). In our new model, we follow the evolution of subhaloes analytically, so we treat the tidal disruption for Type 1s and 2s in the same way. A satellite galaxy (Type 1 or Type 2) will be disrupted by the tidal force of the main halo, when 1) it has more baryonic matter than dark matter ($M_{\text{bar}} > M_{\text{sub}}$); 2) its average baryonic mass density is lower than main halo density at the peri-centre of its orbit.

2.3 The physical prescriptions for ram pressure stripping of cold gas

In the L-Galaxies model, ram pressure strips only the hot gas component in the satellite galaxies, while the cold gas component in the ISM is not affected. Following the prescriptions of Gunn & Gott (1972), we consider a satellite galaxy moving through its host halo. The RP force can be written as,

$$P_{\text{r,p}}(R) = \rho_{\text{ICM}}(R)v^2 \quad (11)$$

where v is the orbital velocity of the satellite, which we take to be the virial velocity of its parent halo. ρ_{ICM} is the density of the hot gas of the parent halo as Eq.(4). When the ram pressure exceeds the interstellar pressure P_{ISM} , cold gas will be stripped. We adopt the Eq.(12) given by Tecce et al.(2010):

$$P_{\text{ISM}} = 2\pi G \Sigma_{\text{disc}}(r) \Sigma_{\text{gas}}(r) \quad (12)$$

where r is the radius to the centre of satellite. Σ_{disc} is the surface density of the galactic disc, which equals to the sum of the cold gas and stellar surface densities:

$$\Sigma_{\text{disc}} = \Sigma_{\star}(r) + \Sigma_{\text{gas}}(r) \quad (13)$$

We calculate P_{ISM} in each radial concentric ring in satellite galaxies based on the division of the disk into multiple rings introduced in the Fu13 model. In our model, the cold gas in a satellite galaxy can be stripped by RP only when the satellite falls within the virial radius R_{vir} of the central galaxy and $P_{\text{r,p}}(R) \geq P_{\text{ISM}}(r)$. The stripped cold gas of the satellite is added to the hot gas component of its central galaxy. According to Eq. (11) & (12), the criterion for

RP stripping for a satellite galaxy at the distance R to the centre of its parent halo is written as:

$$2\pi G [\Sigma_{\star}(r) + \Sigma_{\text{gas}}(r)] \Sigma_{\text{gas}}(r) \leq \rho_{\text{ICM}}(R) v^2 \quad (14)$$

From the radial distribution of cold gas $\Sigma_{\text{gas}}(r)$ and stellar surface density $\Sigma_{\star}(r)$, we evaluate the stripping radius r in Eq. (14) and assume that cold gas exterior to this radius r will be stripped.

The above description is very simplistic. It is not clear if all the cold gas will be stripped immediately when the RP force is larger than the gravity of the satellite itself. To take account of this uncertainty, we define a stripping fraction f_{rps} as the fraction of the cold gas stripped by ram pressure in the region of a satellite galaxy where $P_{\text{r,p}}(R) \geq P_{\text{ISM}}(r)$. In the simplest case, f_{rps} is 100%, which means all the cold gas in the region where $P_{\text{r,p}}(R) \geq P_{\text{ISM}}(r)$ will be stripped by RP. This simple assumption causes a sudden cut off of the cold gas radial profile, i.e the cold gas radial profile becomes a step function at the radius r . To ensure a continuously decreasing cold gas radial profile, we modify the stripping law as follows : if $P_{\text{r,p}} \geq P_{\text{ISM}}$, the stripping ratio f_{rps} is related to the difference between $P_{\text{r,p}}$ and P_{ISM} as:

$$f_{\text{rps}} = \begin{cases} 0, & P_{\text{r,p}} < P_{\text{ISM}} \\ \frac{P_{\text{r,p}} - P_{\text{ISM}}}{P_{\text{r,p}}}, & P_{\text{r,p}} \geq P_{\text{ISM}} \end{cases} \quad (15)$$

The guarantees that only part of the cold gas $M_{\text{stripped}} = f_{\text{rps}} M_{\text{coldgas}}(r)$ in the region where $P_{\text{r,p}}(R) \geq P_{\text{ISM}}(r)$ will be stripped.

3 PERFORMANCE OF THE NEW MODEL

In this section, we compare our new model with the Fu13 model and explore if we obtain more convergent and/or improved results for the following galaxy properties: the stellar/gas mass function and the two-point correlation function. These two quantities are often used as basic tests of the overall model. We then study the fraction of quenched galaxies as a function of halo mass and compare with observational data. In the following subsections, we abbreviate our model as “new” if the option for cold gas stripping is switched off, and it is labeled as “new +rps” if the cold gas stripping is turned on.

3.1 The stellar and cold gas mass functions

In Fig. 1, we plot the model mass functions of stars, HI and H_2 at $z = 0$ compared with the observations. The “new” model results (with RP stripping of cold gas off) are shown as black and blue lines for the MS and MS-II simulations, respectively. All the free parameters of the models are fixed as in Fu13 (see the Table 1. in that paper), with the exception of the hot gas accretion efficiency onto black holes κ_{AGN} which is changed from $1.5 \times 10^{-5} M_{\odot} \text{yr}^{-1}$ to $1.5 \times 10^{-6} M_{\odot} \text{yr}^{-1}$. Tuning this parameter is necessary in order to better fit the stellar mass function at the high mass end. As can be seen, with this minor change, our new models are in very good agreement with the observational data at $z = 0$ for both simulations.

Fig. 1 also shows that there is difference in the predicted mass functions at the low-mass end between the two

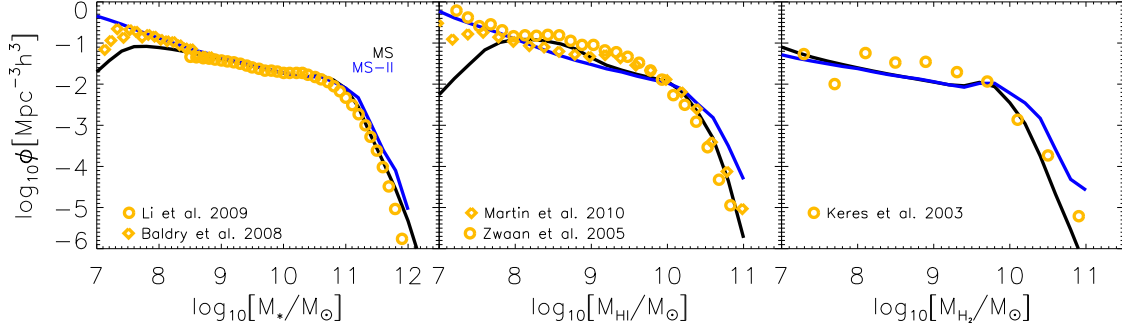


Figure 1. The stellar, HI and H₂ mass functions at $z = 0$ from the new model compared with observations. The solid curves show results for the new model without the process of ram pressure stripping of cold gas. Blue and black curves show results for generated from the MS and MS-II simulations, respectively. For the observations, stellar mass functions are from Li & White (2009) and Baldry et al. (2008); the HI mass functions are from Zwaan et al. (2005) and Martin et al. (2010) a the; H₂ mass function is from Keres et al. (2003).

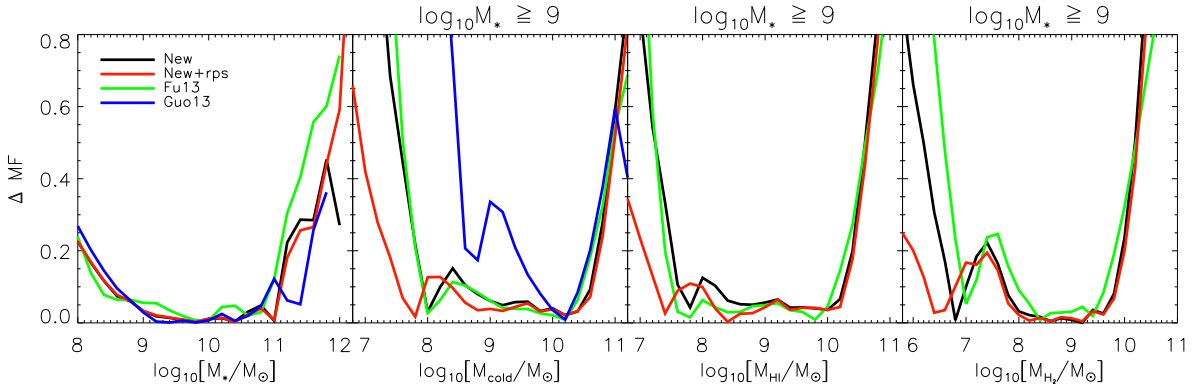


Figure 2. Convergence check: the difference of the predicted stellar, cold gas, HI and H₂ mass functions between MS and MS-II. The black/red lines are for our new model without/with ram pressure stripping of cold gas. The green/blue lines are for the Fu13 and Guo13 models.

simulations. In Fig. 2, we check the divergence between two simulations in detail, where the difference defined as $\Delta MF = |\log_{10} MF_{MS} - \log_{10} MF_{MS-II}|$. The left panel shows that for low-mass galaxies ($\log_{10} M < 8.5$) there is obvious difference in the mass function, and all the models have similar predictions (also see Fig.7 in Guo11). Such a difference is expected and it is basically due to low-mass central galaxies not being resolved in the low-resolution simulation. In fact the simulation resolution can have more complicated effects on the galaxy properties. For example, if the merger trees of some massive halos in the MS simulation are not well-resolved at higher redshifts, this will lead to divergence in the properties of both the central and the satellite galaxies in those halos. Overall we find that the stellar mass function is more convergent for galaxies with $\log_{10} M_* > 8.5$ and in our later analysis we only focus on these galaxies.

The right panels of Fig. 2 show the convergence test on the cold gas mass functions, also divided into HI and H₂ components. The sample is selected with $\log_{10} M_* > 9$. It is found that, compared to the Guo11 model, our new model

produces more convergent results for the cold gas mass. In the Guo11 model, there is a threshold in cold gas mass for star formation which implies that all satellite galaxies contain cold gas even when they stop forming stars. In a low-resolution simulation, the satellite will soon become type 2 and gas cooling will stop as the hot halo gas is immediately stripped. So there will be more cold gas in the low-resolution run for the Guo11 model. Compared to the Fu13 model on which our model is based, it is seen that our new model does not produce a more convergent results on the cold gas and HI gas mass, but we obtain slightly better convergence on the H₂ mass (right panel), and the convergence is more obvious in our new+rps model.

In Fig. 3 we further check the convergence in different halo mass bins. It is clearly seen that the convergence in the new model is better at $10^7 M_{\odot} < M_{H_2} < 10^{10} M_{\odot}$ than the Fu13 model. The new+rps will mostly affects the low-mass end ($< 10^7 M_{\odot}$) as rps is efficient to strip the cold gas if there is little of it. In the Fu13+rps model, the H₂ mass function is converged only at the low-mass end, but not at

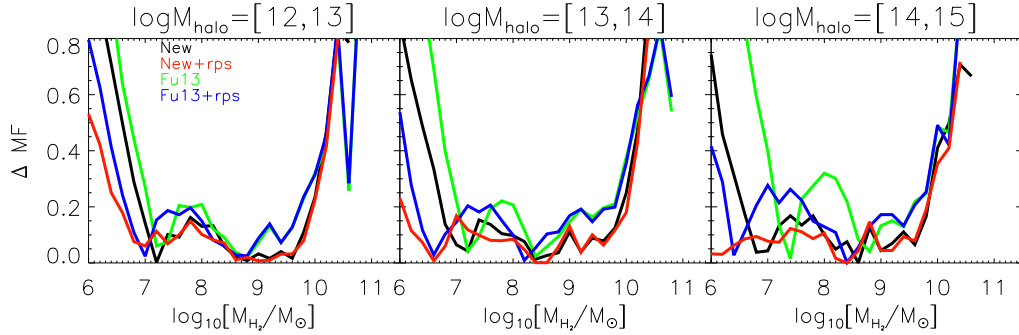


Figure 3. Convergence check: the difference of the predicted H_2 mass functions of the satellites ($\log M_* > 9.5$) in different halo mass bins between MS and MS-II. The black/red lines are for our new model without/with ram pressure stripping of cold gas. The green/blue lines are for the Fu13 and Fu13+rps models. More obvious improvement in convergence is seen in massive haloes.

the high-mass end. This plot clearly shows that without a sub-resolution treatment of the star formation physics (such as Fu13 model), it is difficult to achieve convergence in high-mass H_2 galaxies and rps is effective in convergence in low gas-mass galaxies. As in the Fu13 and our model, the star formation is determined by local H_2 gas density, it is expected that our model will produce more convergent results on the fraction of passive/star forming galaxies, and this is shown in detail in Sec.3.3.2.

3.2 The projected two-point correlation functions (2PCF)

The two-point correlation function (2PCF) is another important galaxy statistic, because it describes how galaxies are distributed in and between dark matter haloes. On small scales, the clustering depends strongly on how satellites are distributed in massive haloes, so it is interesting to ask if the model results are dependent on simulation resolution. Another reason to check the 2PCF is that, as shown by Kang (2014), strong SN feedback in satellites can decrease the 2PCF on small scales, and this results in better agreement with the observations. Our new model also includes a feedback model similar to Kang (2014) for satellite galaxies, in which the feedback efficiency depends on the local gravitational potential of the satellite. It is thus worthwhile to check if our new model can give better agreement with the observed 2PCFs.

In Fig. 4, we plot the projected galaxy 2PCFs for the Fu13 model in green and for our new model in black. Results are plotted for both the MS and MS-II simulations and the difference between the two is shown as in inset at the bottom of each panel. The different panels show results for galaxies in different bins of stellar mass. The data points are from Li et al. (2006) and are computed using the large-scale structure sample from the SDSS DR7. Here we do not show the results from the “new+rps” – the results are very similar to the model without cold gas stripping.

Fig. 4 shows that our new model produces better agreement with the observed 2PCFs compared to the Fu13 model, especially for low-mass galaxies. As discussed in the previous section, our new model employs a feedback prescription where the SN ejection efficiency is dependent on V_{max}

of the subhalo, and not the central halo, as in previous models. So the feedback efficiency in satellites in our new model is larger, and this decreases the mass growth of satellites after infall with respect to the results of Fu13. As shown by Kang (2014), strong feedback in satellites flattens the satellite galaxy mass function in massive haloes, thus reducing the clustering amplitude on small scales.

The panel inserts show that the disparity in clustering amplitude between the MS and MS-II simulations is slightly lower in the new model compared to Fu13 model. The new model shows a little “better” convergence at small scales, but in some mass bins new model get “worse” at \sim Mpc scales. However, these difference on 2PCFs between the two simulations is always small (often lower than 0.2 dex), indicating that resolution is not of primary importance in the prediction of galaxy clustering.

In Fig. 5 we show 2PCFs for galaxies classified into red and blue according to their $g-r$ colors as described in Guo11. The red/blue lines are model predictions for red/blue galaxies, and the red/blue points are data points from Li et al. (2006). As shown in the previous figure, the difference between the MS and MS-II simulations are small for 2PCFs, so we only show results from the MS. The new model fits better the color-dependent clustering in low-mass bins, particularly for blue galaxies in the low mass bins. In intermediate mass bins ($\log M_* = [9.77, 10.77]$) the clustering of red galaxies is too strong, and too low for blue galaxies for both models. This is because both the Fu13 and our models over-predict the fraction of red satellite galaxies and under-predict the fraction of red centrals, as seen in Fig.8. Both models also fit well at the highest stellar masses.

3.3 Satellite quenching and cold gas depletion

In this subsection, we will investigate the effects of RP stripping of cold gas in galaxies. We will study how ram-pressure stripping changes the quenched fraction of galaxies as a function of galaxy mass, halo mass and cluster-centric radius, and we will also show comparisons with recent observations. As in the previous subsections, we will also address the issue of convergence by showing results from both the MS and the MS-II simulations.

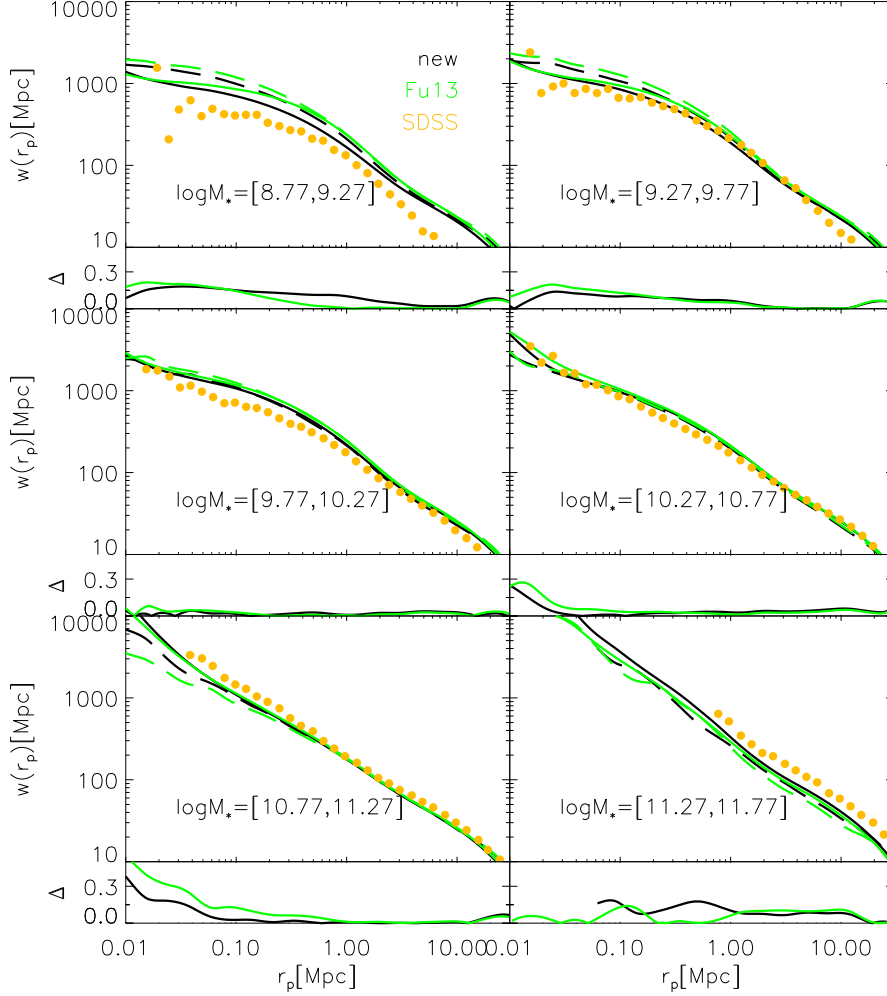


Figure 4. The projected 2PCFs for galaxies in different stellar mass bins (top graph in each panel) and absolute values of difference of the amplitude of the 2pcfs between MS and MS-II, $\Delta = |\log_{10} w_{\text{MS}} - \log_{10} w_{\text{MS-II}}|$ (lower graph in each panel). The results from MS are shown with solid lines, and those from MS-II are shown using dashed lines. Black curves show results for our new models and green curves show results for the Fu13 models. The orange dots are data from SDSS. Here we only show the results from our new model without RP stripping of cold gas.

3.3.1 Where is ram-pressure stripping most effective?

To understand which galaxies have been affected most by ram-pressure stripping, we define the cumulative stripped cold gas fraction as

$$f_{\text{sp}} = \frac{M_{\text{asp}}}{M_{\text{asp}} + M_{\text{coldgas}}} \quad (16)$$

where M_{asp} is the cumulative mass of stripped cold gas throughout the formation history of a galaxy (evaluated by summing up the stripped cold gas mass in the main progenitor), and M_{coldgas} is its current cold gas mass. We focus on satellite galaxies in rich groups and clusters, and select those with $M_* > 10^9 M_\odot$ in haloes with mass $M_{\text{halo}} > 10^{13} M_\odot$.

Fig.6 shows the fraction of galaxies with f_{sp} larger than a certain value x ($0.1 < x < 1.0$). Results are shown for

both MS and MS-II haloes and are seen to agree to within $\sim 10\%$. We find that about 50% galaxies in massive haloes have $f_{\text{sp}} \geq 0.1$. We then define a galaxy with $f_{\text{sp}} \geq 0.1$ as having had significant cold gas stripping, and we plot the fraction of these galaxies $N_{\text{stripping}}/N_{\text{total}}$ as functions of stellar mass and halo mass in Fig.7. As can be seen, the fraction of galaxies with significant stripping increases steeply with halo mass, but decreases with stellar mass.

If we increase the significant stripping threshold from 0.1 to 0.5, we find that the stripped fraction in haloes of $10^{13} M_\odot$ decreases from 0.6 to 0.2. Brüggen & De Lucia (2008) found that about one quarter of galaxies in massive clusters ($M_{\text{halo}} > 10^{14} M_\odot$) are subjected to strong ram pressure that causes loss of all gas and more than 64% of galaxies that reside in a cluster today have lost substantial gas. Our

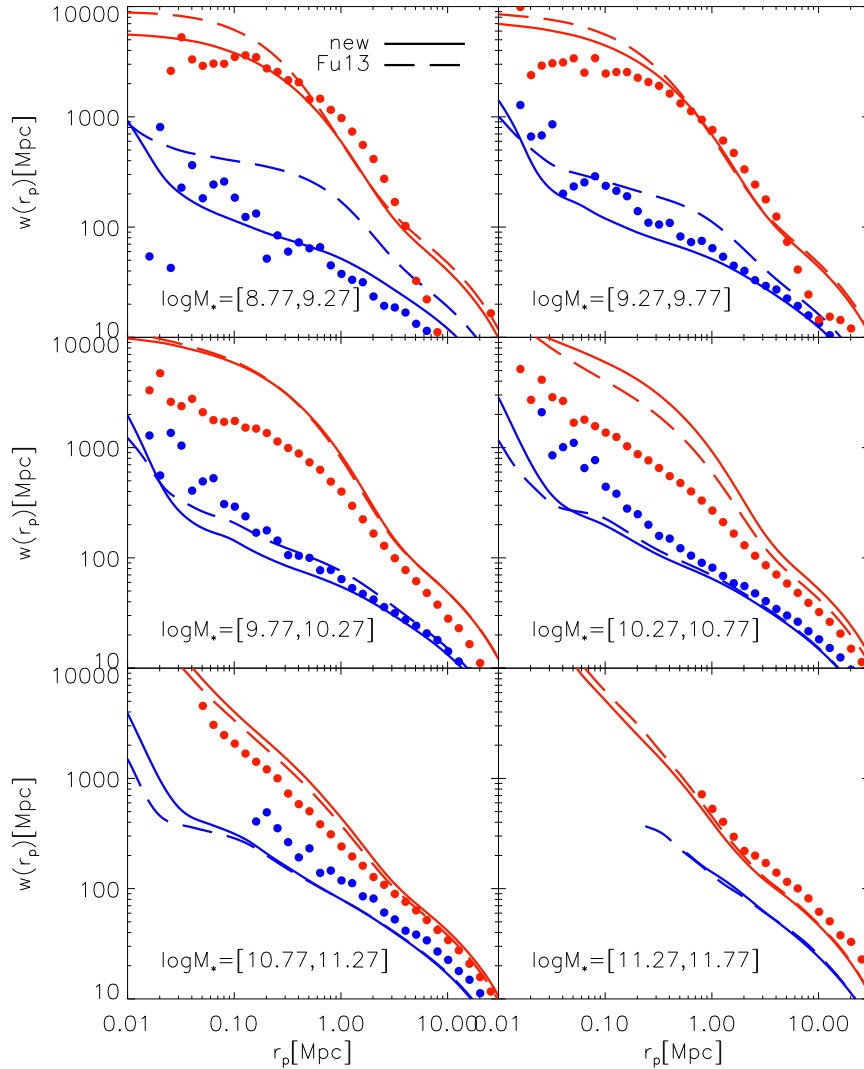


Figure 5. As in Fig. 4, but separately for red and blue galaxies.

new model agrees well with these results. We also conclude that most low-mass satellite galaxies in massive clusters will lose significant fraction of their cold gas by RP stripping, and some will lose all their interstellar cold gas.

3.3.2 Effect of ram-pressure stripping on the quenched fraction of satellite galaxies

The fraction of quenched galaxies is known to depend on environment. It has also been shown (e.g., Weinmann et al. 2006) that early versions of SAMs (e.g., Croton et al. 2006) over-predicted the fraction of red satellites in all environments. It was suggested that instantaneous stripping of the hot halo gas of satellites was to blame. By introducing a non-instantaneous stripping model, later SAMs (e.g., Kang & van den Bosch 2008; Font et al. 2008) were able to produce more blue galaxies, but the agreement was still not satisfactory. In the Guo11 and Fu13 models, the stripping of hot halo gas is modeled as a gradual process. Recently Henriques

et al. (2015) showed that the latest version of L-Galaxies was able to reproduce the overall red galaxy fraction, but they did not analyze central/satellite galaxies separately, nor did they examine the dependence of red fraction on halo mass and radial distance from the centres of groups and clusters.

Wetzel et al. (2012) re-analyzed the fraction of quenched galaxies in groups and clusters using SDSS DR7 data. They classified galaxies as quenched based on their specific star formation rates rather than their colors. This permits a more direct comparison with models, because the galaxy color is a complicated function of star formation history, metallicity and dust extinction. The analysis of Wetzel et al. (2012) made use of global star formation rates with fibre aperture correction as given in Salim et al. (2007). These corrections may be prone to systematic effects, because there can be a large spread in broad-band colors at a given specific star formation rate and because the corrections are calibrated using average relations between these two quantities. The corrections also account for two thirds of the total star for-

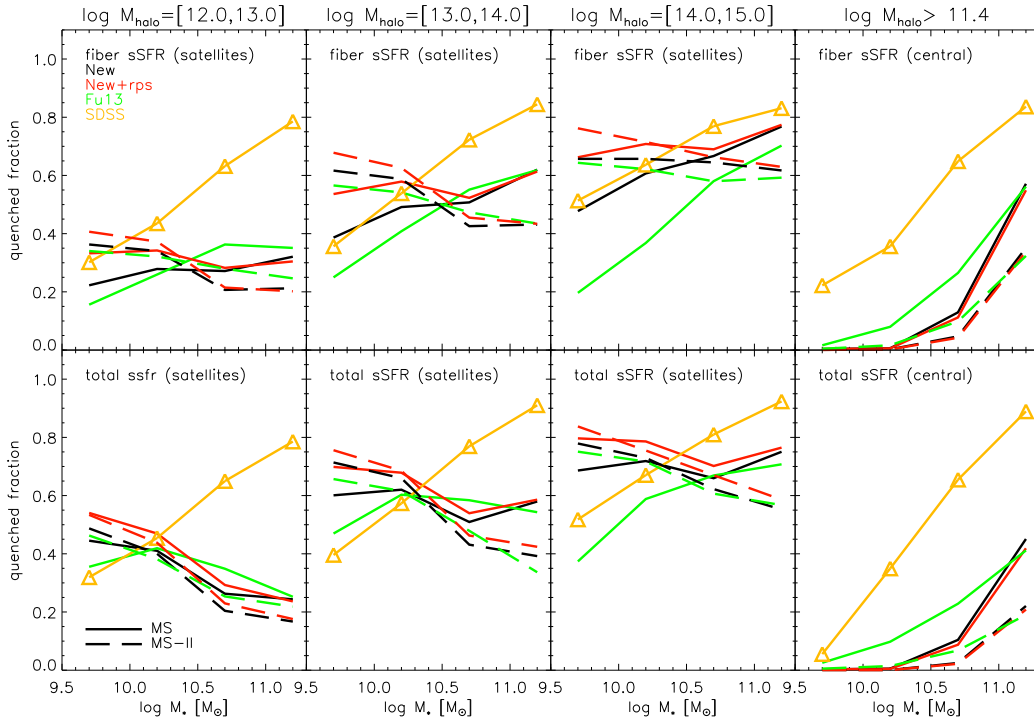


Figure 8. The quenched fraction of galaxies as a function of stellar mass: the left three columns are for satellite galaxies in different halo mass bins, and the right column is for central galaxies in all haloes with masses greater than $10^{11.4} M_{\odot}$. The top panels show results when quenched galaxies are defined using sSFRs measured within the SDSS fiber, and the lower panels show results when corrected total star formation rates are used instead. In each panel, the triangles are the SDSS data and the colored lines are different model predictions (solid for MS, dashed for MS-II results).

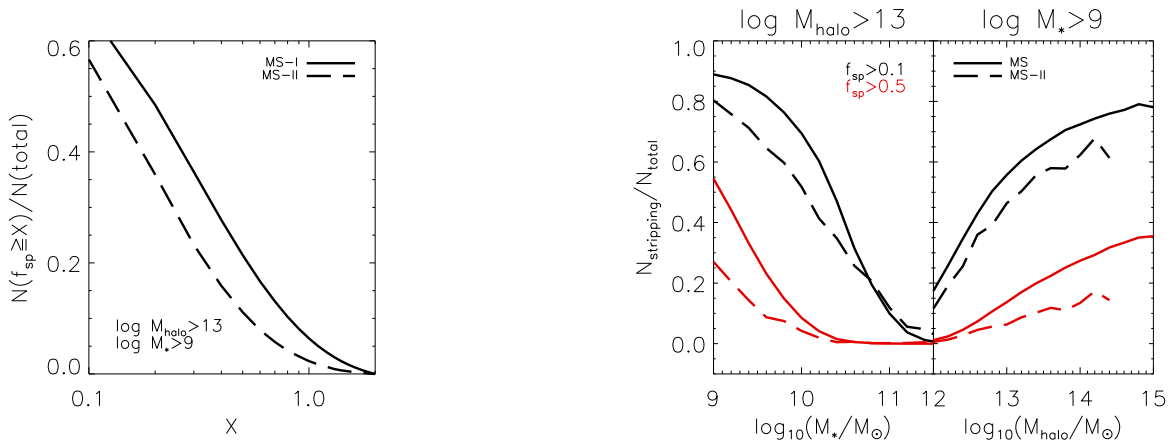


Figure 6. The fraction of galaxies with stripping fraction $f_{sp} \geq x$ as a function of x . Solid and dashed lines are based on MS and MS-II haloes respectively. Here galaxies are selected with stellar mass $M_* > 10^9 M_{\odot}$ in haloes with $M_{halo} > 10^{13} M_{\odot}$.

Figure 7. The number fraction of galaxies with $f_{sp} > 0.1$ (black curves) and $f_{sp} > 0.5$ (red curves) as a function of stellar mass and halo mass. Solid and dashed lines are based on MS and MS-II haloes respectively.

mation rate on average. In contrast, the star formation rate measured inside the fiber aperture is derived directly from the dust-corrected H α luminosity and should be more reliable. In the following comparison, we present the results on quenched fractions using both total and fiber aperture specific star formation rates. We also examine the radial

dependence of the quenched fraction in different halo mass bins.

Following the same procedure described in Wetzel et al. (2012), we extract galaxies from the MPA-JHU SDSS DR7 catalogue with $M_* > 10^{9.5} M_{\odot}$ at $z < 0.04$ and $M_* > 10^{9.5} M_{\odot}$ at $z = 0.04 \sim 0.06$ that are included in the group

catalogue of Yang et al.(2007). We use the stellar masses, the fibre sSFRs (specific star formation rates) and total sSFRs from the MPA-JHU SDSS DR7 database. Following Wetzel et al., we define galaxies with $sSFR < 10^{-11} \text{yr}^{-1}$ as quenched galaxies, and calculate the quenched fraction of satellite galaxies in different bins of halo mass, stellar mass and cluster-centric radius, scaled to the virial radius of the halo. We find that f_Q^{sat} increases with the stellar mass of the satellite, host halo mass and distance to the center of the halo and our results are largely consistent with those presented in Wetzel et al.(2012) (see Fig. 8 to 10).

In the models, we select galaxies with $M_* > 10^{9.5} M_\odot$ at $z = 0$ from the MS and MS-II simulations. We use the FOF halo properties given by the N-body simulation to define the halo mass. However, in order to account for projection effects in the simulation, we convert 3D distances to 2D distances by simply projecting the galaxies onto the X-Y plane in the simulations and selecting galaxies within $\Delta V_z \leq 500 \text{km/s}$ to the halo central as group members. This is a reasonably close representation of the Yang et al. (2007) procedure to select galaxy groups in redshift space.

In Fig. 8 and Fig. 9, we show the quenched fraction of satellite galaxies as function as their stellar mass in a set of different halo mass bins, and as a function of host halo mass in a set of different stellar mass bins. In Fig. 8, we also show the quenched fraction of central galaxies in all haloes with $\log M_{\text{halo}} > 11.4$ in the right panel. In both figures, results from our new model without ram-pressure stripping are shown in black, from our new model with cold gas stripping in red, and from Fu13 in green. The solid lines are results from the MS, and the dashed lines are for the MS-II simulation. The yellow triangles show the SDSS results. In each figure, we plot the results for fiber sSFRs in the upper panels, and for total sSFRs in the lower panels. At our median redshift, the 3 arcsec aperture of the fiber corresponds to a physical aperture size of $1.5 \text{kpc}/h$.

One important conclusion from these two figures is that our new models (w/o RP stripping) produce much more convergent results between the two simulations than the Fu13 model, particularly for low-mass satellite galaxies. For example, in the upper middle two panels of Fig. 8 the predicted quenched fractions at low stellar masses differ by factors of 2-3 between the MS and MS-II for the Fu13 models, but improved to within a factor of 1.5 in our new models. In the $\log M_{\text{halo}} = [14, 15]$ panel, as we discussed in Sec. 3.1, the convergence is more obviously in the new model. The same is seen in the leftmost panel of Fig. 9 and for the highest halo mass bins in Fig. 10.

We also conclude that the predictions using the fiber and total sSFR are qualitatively very similar. There are significant discrepancies between all the models and the observations which are much larger than any of the systematics in the way we choose to define the boundary between quenched and actively star-forming galaxies. The clear *qualitative* discrepancies are the following:

- (i) The rightmost panel of Fig. 8 shows that the quenched fraction of central galaxies is lower than the data, across all stellar masses. This under-prediction of red centrals agrees with previous results based on galaxy color (e.g., Weinmann et al. 2006; Kang et al. 2006).
- (ii) Comparing Fig. 8 and 9, we see that in the data, the

quenched fraction depends on both stellar mass and on halo mass. At fixed halo mass, there is still a strong dependence of quenched fraction on the stellar mass of the galaxy. At fixed stellar mass, there is a significantly weaker dependence of quenched fraction on halo mass. This indicates that halo mass has *secondary* influence on the star formation histories of galaxies compared to stellar mass.

In the models, the *opposite* is true. At fixed halo mass, there is generally only a weak dependence of the quenched fraction on stellar mass. At fixed stellar mass, the dependence of the quenched fraction on halo mass is very strong. This indicates that in the models, the influence of the halo mass on star formation history is *primary* and the influence of stellar mass is secondary.

As we will discuss in the final section, our results indicate that the physical model for determining the star formation histories of galaxies in the SAMs must be wrong.

In Fig. 10, we show the relation between the quenched satellite fraction and the projected distance to the center of the scaled by R_{200} . Results are shown in 3 halo mass bins. Once again we see that the new models produce results that are much less sensitive to resolution than than Fu13 models. As can be expected from the results in the previous two figure, there are clear offsets between the quenched fractions in the models and the data. The slope of the decrease in quenched fraction as a function of scaled radius agrees quite well with the observations in high mass haloes. In low mass haloes, the quenched fraction rise too steeply near the center. The steep rise towards the center is stronger for the total specific star formation rates compared to the fibre specific star formation rates, and it is also stronger for the model that includes ram-pressure stripping of the cold gas. This suggests that the central density of hot gas in lower mass haloes is too high or our rps model is too simple. Future constraints can be obtained from hydrodynamical simulations and the observed HI map of galaxies.

In summary, we conclude that our models greatly alleviate the resolution problems seen in the Fu13 models, but are still in significant discrepancies with the observational data remain.

3.4 Comparison of the dependence of HI fraction and sSFR on environmental density

In this section, we compare model predictions of the HI mass fractions of galaxies as a function of environmental density to observations in order to test our models of ram-pressure stripping. Using the observational data from a few combined surveys (ALFALFA, GALEX, SDSS), Fabello et al. (2012, hereafter Fabello12) found that both the HI fractions and sSFRs of low-mass galaxies decline with increasing environmental density, but the HI fraction exhibits a steeper decline. They compared the data with the results of the Guo11 model, and found that this model predicts the opposite effect – the sSFRs decline more steeply with density than the HI mass fractions.

Following Fabello12, we select galaxies with $9.5 < \log(M_*/M_\odot) < 11$, and compute the environmental density parameter N , defined as the number of neighbours with $\log(M_*/M_\odot) \geq 9.5$ located inside a cylinder of 1Mpc in projected radius and with velocity difference less than 500km/s .

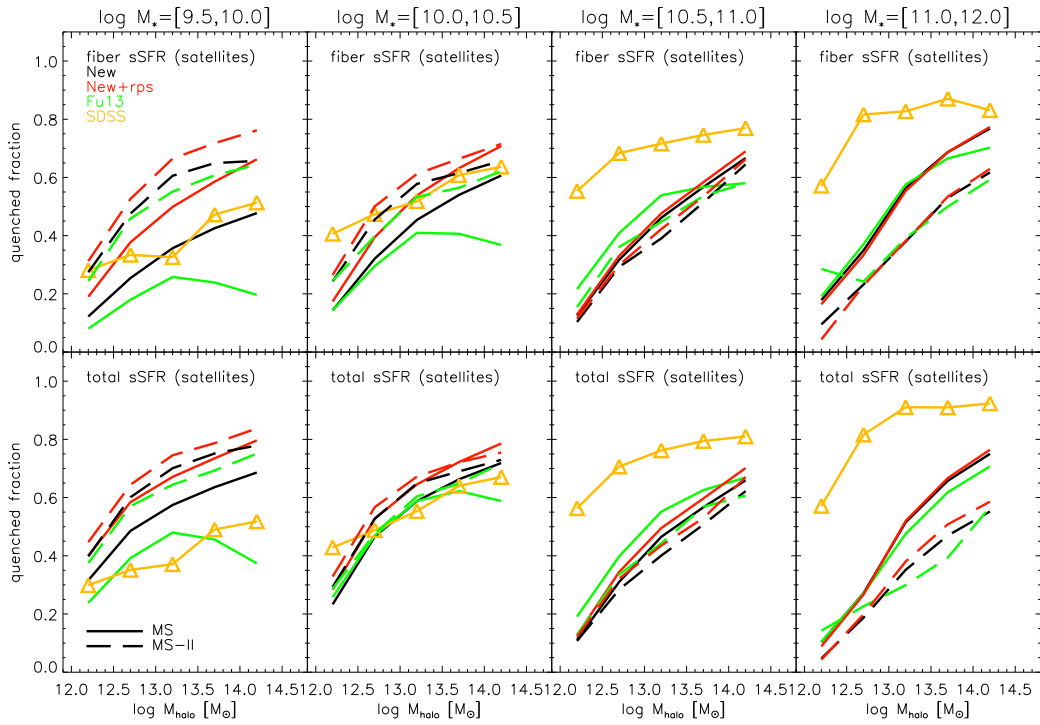


Figure 9. As in Fig. 8, but now quenched fractions are plotted as a function of halo mass in different stellar bins.

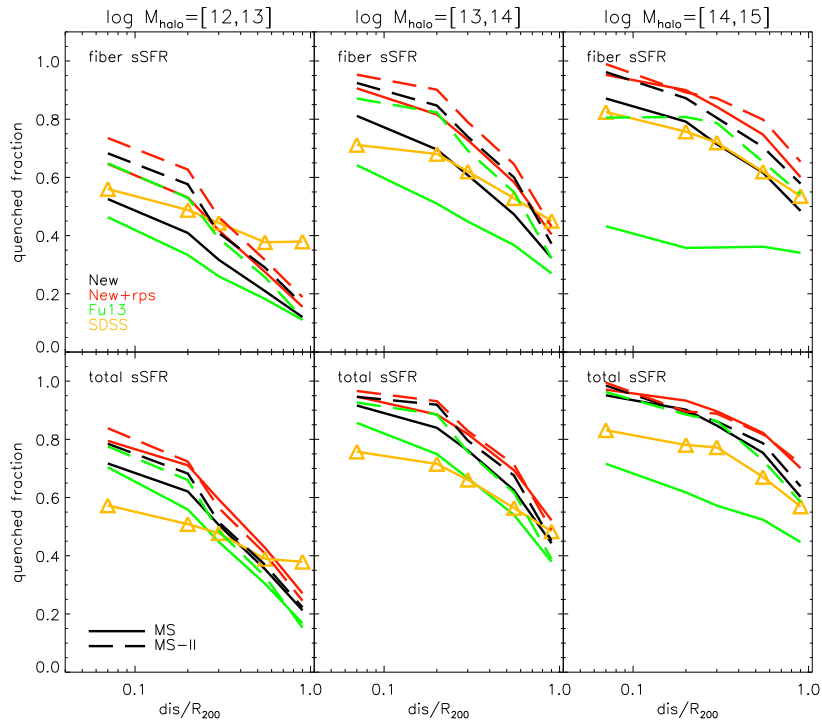


Figure 10. The quenched satellite fraction versus the projected distance to the centre of the halo scaled by the virial radius of the halo. Results are shown in 3 different halo mass bins.

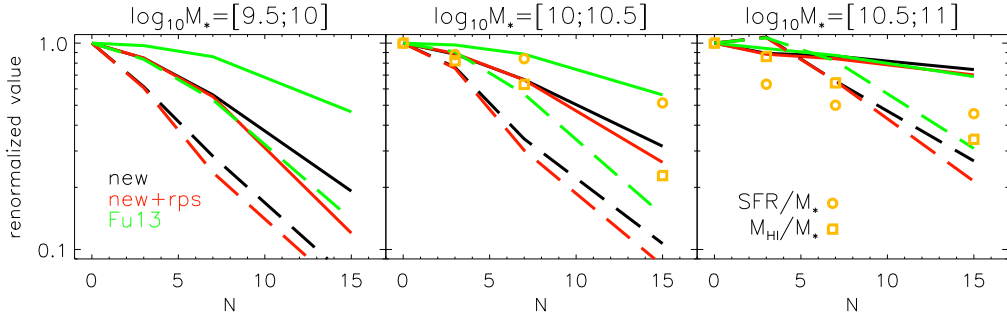


Figure 11. The relations between the values of M_{HI}/M_* and sSFR renormalized to 1 at $N=0$ as a function of N , where N is the environmental parameter (see text for details). Results are shown in two different stellar mass bins. The right two panels also show data from Fabello et al. 2012. The lines are model predictions, with solid lines indicating results for fibre sSFR, and dashed lines indicating results for HI mass fraction .

The comparison between models and data is shown in Fig. 11. All curves have been normalized to 1 at $N=0$, and the *relative* decrease in SFR/M_* and M_{HI}/M_* is plotted on the y-axis. The mass bins have been chosen to match the stellar mass bins shown in Fabello12.

Unlike the Guo11 model, the the HI mass fraction declines with density more rapidly than the specific star formation rate for the Fu13 and for the new models. The reason for this is because in the Guo11 models, star formation ceases in the whole galaxy when the cold gas mass is lower than a threshold value. This has the consequence that significant gas always remains in passive galaxies. In the Fu13 and our new models, the local star formation rate is determined purely by the local gas surface density. As can be seen by comparing the red and the black curves, the inclusion of ram-pressure stripping processes enhances the the decline in HI mass fraction at large N , by only a small factor, indicating that the star formation prescription rather than the treatment of stripping is more important in understanding the observational results.

A more comprehensive test of our ram-pressure stripping prescriptions requires HI observations of galaxies near the cores of galaxy groups and clusters.

4 CONCLUSION AND DISCUSSION

The main results and findings of this paper can be summarized as follows:

- (I) We include an analytic method to trace the properties of the subhaloes of satellite galaxies in haloes that is independent of the resolution of the simulation. This allows us to write down equations describing the physical processes such as SN feedback, gas cooling, gas reincorporation and tidal stripping that are not sensitive to whether the galaxy is classified as a Type 1 or Type 2 galaxy in the simulation. The predicted gas mass functions, quenched satellite fractions and galaxy two-point correlation functions evaluated for the two simulations used in this work, MS and MS-II, agree better than in previous models.
- (II) We include a new prescription to describe the ram pressure stripping of cold gas in the galaxy.

We then compare a variety of results with recent observations. Our main conclusions are the following:

- (i) Our new models allow for continued gas accretion and SN feedback in all satellite galaxies. We improved the H_2 convergence for satellites in massive haloes which leads to more convergent quenched fraction of satellites in mass haloes. This has the effect of decreasing the clustering amplitude of low mass galaxies on small scales, resulting in a slightly better agreement with the observed 2pcf compared to previous models.
- (ii) We show that ram pressure stripping is most efficient at removing the cold gas from low mass satellite galaxies ($< 10^{10.5} M_\odot$) in massive haloes ($> 10^{13} M_\odot$). More than 60% of the galaxies in these massive haloes have experienced significant ram-pressure stripping.
- (iii) We study the quenched fraction of satellite galaxies as a function of stellar mass at fixed halo mass, and as a function of halo mass at fixed stellar mass. We find significant discrepancies between our model predictions and observations. At the fixed halo mass, the quenched fraction of satellites does not depend on stellar mass in the models. This is in contradiction with observations where the quenched fraction always increases with stellar mass. The net effect of this discrepancy is that there are too many low mass quenched satellites and too few high mass quenched satellites in the models compared to the data.
- (iv) We study the decrease in the quenched fraction of satellite galaxies as function of of projected radial distance from the center of the halo. The slope of the decrease agrees well with observations in high mass haloes, but is much steeper than observed in low mass haloes. This problem is worse for models that include the ram-pressure stripping of cold gas, indicating that the predicted hot gas densities in the centers of lower mass haloes may be too high.
- (iv) Our new models are able to reproduce the relatively stronger decrease in HI gas mass fraction as a function of local environmental density compared to specific star formation rate first pointed out by Fabello12.

Our study in this paper shows that the long-standing problem of the over-prediction of red satellite galaxies is still not solved in the current version of the L-Galaxies model. Recently Sales et al. (2015) studied the color of satellite

galaxies in the Illustris cosmological simulations. They found that their simulation produces more blue satellites and proposed that the main reason SAMs fail to reproduce satellite colors is that there is too little cold gas in satellites before they are accreted. We regard this scenario as unlikely, because as we have shown, our SAMs produce gas mass functions in excellent agreement with observations at the present day. Fu13 demonstrated that the H_2 mass functions of galaxies evolve very strongly with redshift. Although keeping more cold gas in satellites before accretion could in principle solve the problem of too many red satellites, it would likely violate other observational constraints. Kang (2014) have also shown that the stellar mass growth in satellite galaxies after infall should not be significant, otherwise there would be too many low-mass galaxies in massive clusters, and the clustering amplitude would be too high clustering on small scales. Wetzel et al. (2013) also found from SDSS that the stellar mass growth of satellite galaxies is constrained to be less than 60% on average.

Recently, it has been shown that a large fraction of low mass galaxies do not experience continuous star formation histories, but have undergone a significant bursts of star formation (Kauffmann 2014). What exactly causes these bursts is not yet understood, but in all likelihood all these results indicate that gas accretion processes onto low mass field galaxies are more complex than assumed in the current semi-analytic models. We note that the net effect of a bursty star formation history is to produce a sSFR distribution with a tail that is skewed towards *low specific star formation rates*, because the duty cycle of the burst phase when the galaxy is forming stars very rapidly is short. An extra tail of low sSFR galaxies at low stellar masses would bring the model central galaxy quenched fractions into better agreement with observations, as seen in the rightmost panel of Figure 8. It would also lower the specific star formation rates of a significant fraction of galaxies being accreted as satellites, perhaps causing them to exhaust their existing gas reservoirs more slowly. Another issue that was pointed out in a paper by Kauffmann (2015) is that there is a correlation between low mass galaxies that are quenched and the quenched fraction of their neighbours that extends over very large scales and that is not currently reproduced by semi-analytic models or by the Illustris simulation.

Until we have a model that reproduces basic trends in quenched fractions as a function of both stellar mass and halo mass, it will be difficult to come to robust conclusions as to whether our treatment of ram-pressure stripping of cold gas is a significant improvement to the models. We have presented some tentative evidence that hot gas densities at the centers of lower mass haloes ($\sim 10^{12} M_\odot$) are smaller than predicted by our models, because the quenched fractions at the very centers of these haloes are too high in comparison with observations. One way to reduce the central hot gas densities is through radio AGN feedback processes. In the current implementation of radio AGN feedback, the cooling rate onto the central galaxy is reduced, but the gas distribution remains unaffected, which is not physically reasonable. At this level of detail, however, hydrodynamical simulations may provide a better way forward.

ACKNOWLEDGEMENTS

We thank the anonymous referee for useful comments. We also thank Bruno Henriques, Yannick Bahè, Qi Guo and Simon White for helpful discussions. This work is supported by the 973 program (No. 2015CB857003, 2013CB834900), NSF of Jiangsu (No.BK20140050), the NSFC (No. 11333008, 111303072,U1531123) and the Strategic Priority Research Program the emergence of cosmological structure of the CAS (XDB09000000). YL acknowledges the support and hospitality by the Max-Planck Institute for Astrophysics. JF acknowledges the support by the Opening Project of Key Laboratory of Computational Astrophysics, National Astronomical Observatories, CAS.

REFERENCES

- Abadi M. G., Moore B., Bower R. G., 1999, MNRAS, 308, 947
 Angulo R. E., White S. D. M., 2010, MNRAS, 405, 143
 Baldry I. K., Balogh M. L., Bower R. G., Glazebrook K., Nichol R. C., Bamford S. P., Budavari T., 2006, MNRAS, 373, 469
 Baldry I. K., Glazebrook K., Driver S. P., 2008, MNRAS, 388, 945
 Balogh M. L., Baldry I. K., Nichol R., Miller C., Bower R., Glazebrook K., 2004, ApJ, 615, L101
 Bamford S. P., et al., 2009, MNRAS, 393, 1324
 Bekki K., 2014, MNRAS, 438, 444
 Biermann P., Tinsley B. M., 1975, A&A, 41, 441
 Boselli A., Cortese L., Boquien M., Boissier S., Catinella B., Gavazzi G., Lagos C., Saintonge A., 2014, A&A, 564, A67
 Boselli A., Gavazzi G., 2006, PASP, 118, 517
 Bower R. G., Benson A. J., Malbon R., Helly J. C., Frenk C. S., Baugh C. M., Cole S., Lacey C. G., 2006, MNRAS, 370, 645
 Boylan-Kolchin M., Springel V., White S. D. M., Jenkins A., Lemson G., 2009, MNRAS, 398, 1150
 Brüggen M., De Lucia G., 2008, MNRAS, 383, 1336
 Butcher H., Oemler A., Jr., 1978, ApJ, 219, 18
 Cole S., Lacey C. G., Baugh C. M., Frenk C. S., 2000, MNRAS, 319, 168
 Croton D. J., et al., 2006, MNRAS, 365, 11
 Crowl H. H., Kenney J. D. P., van Gorkom J. H., Vollmer B., 2005, AJ, 130, 65
 De Lucia G., Blaizot J., 2007, MNRAS, 375, 2
 Dressler A., 1980, ApJ, 236, 351
 Fabello S., Kauffmann G., Catinella B., Li C., Giovanelli R., Haynes M. P., 2012, MNRAS, 427, 2841
 Font A. S., et al., 2008, MNRAS, 389, 1619
 Fu J., Guo Q., Kauffmann G., Krumholz M. R., 2010, MNRAS, 409, 515
 Fu J., et al., 2013, MNRAS, 434, 1531
 Gunn J. E., Gott J. R., III, 1972, ApJ, 176, 1
 Guo Q., White S., 2014, MNRAS, 437, 3228
 Guo Q., White S., Angulo R. E., Henriques B., Lemson G., Boylan-Kolchin M., Thomas P., Short C., 2013, MNRAS, 428, 1351
 Guo Q., et al., 2011, MNRAS, 413, 101
 Haynes M. P., Giovanelli R., 1984, AJ, 89, 758

- Henriques B. M. B., White S. D. M., Thomas P. A., Angulo R., Guo Q., Lemson G., Springel V., Overzier R., 2015, *MNRAS*, 451, 2663
- Hughes T. M., Cortese L., 2009, *MNRAS*, 396, L41
- Jiang F., van den Bosch F. C., 2014, arXiv, arXiv:1403.6827
- Kang X., 2014, *MNRAS*, 437, 3385
- Kang X., Jing Y. P., Mo H. J., Börner G., 2005, *ApJ*, 631, 21
- Kang X., Jing Y. P., Silk J., 2006, *ApJ*, 648, 820
- Kang X., van den Bosch F. C., 2008, *ApJ*, 676, L101
- Kauffmann G., White S. D. M., Guiderdoni B., 1993, *MNRAS*, 264, 201
- Kauffmann G., 2015, *MNRAS*, 450, 618
- Kauffmann G., 2014, *MNRAS*, 441, 2717
- Kauffmann G., Colberg J. M., Diaferio A., White S. D. M., 1999, *MNRAS*, 303, 188
- Kauffmann G., White S. D. M., Heckman T. M., Ménard B., Brinchmann J., Charlot S., Tremonti C., Brinkmann J., 2004, *MNRAS*, 353, 713
- Kenney J. D. P., van Gorkom J. H., Vollmer B., 2004, *AJ*, 127, 3361
- Kimm T., et al., 2009, *MNRAS*, 394, 1131
- Lanzoni B., Guiderdoni B., Mamon G. A., Devriendt J., Hatton S., 2005, *MNRAS*, 361, 369
- Li C., Kauffmann G., Fu J., Wang J., Catinella B., Fabello S., Schiminovich D., Zhang W., 2012, *MNRAS*, 424, 1471
- Li C., Kauffmann G., Jing Y. P., White S. D. M., Börner G., Cheng F. Z., 2006, *MNRAS*, 368, 21
- Li C., White S. D. M., 2009, *MNRAS*, 398, 2177
- Machacek M., Jones C., Forman W. R., Nulsen P., 2006, *ApJ*, 644, 155
- McCarthy I. G., Frenk C. S., Font A. S., Lacey C. G., Bower R. G., Mitchell N. L., Balogh M. L., Theuns T., 2008, *MNRAS*, 383, 593
- Navarro J. F., Frenk C. S., White S. D. M., 1996, *ApJ*, 462, 563
- Okamoto T., Nagashima M., 2003, *ApJ*, 587, 500
- Onions J., et al., 2012, *MNRAS*, 423, 1200
- Roediger E., Hensler G., 2005, *A&A*, 433, 875
- Roediger E., Brüggén M., 2007, *MNRAS*, 380, 1399
- Sakelliou I., Acreman D. M., Hardcastle M. J., Merrifield M. R., Ponman T. J., Stevens I. R., 2005, *MNRAS*, 360, 1069
- Sales L. V., et al., 2015, *MNRAS*, 447, L6
- Salim S., et al., 2007, *ApJS*, 173, 267
- Solanes J. M., Manrique A., García-Gómez C., González-Casado G., Giovanelli R., Haynes M. P., 2001, *ApJ*, 548, 97
- Somerville R. S., Primack J. R., 1999, *MNRAS*, 310, 1087
- Springel V., et al., 2005, *Natur*, 435, 629
- Springel V., White S. D. M., Tormen G., Kauffmann G., 2001, *MNRAS*, 328, 726
- Tecce T. E., Cora S. A., Tissera P. B., Abadi M. G., Lagos C. D. P., 2010, *MNRAS*, 408, 2008
- Tonnesen S., Bryan G. L., 2012, *MNRAS*, 422, 1609
- Tonnesen S., Bryan G. L., 2009, *ApJ*, 694, 789
- Tonnesen S., Bryan G. L., 2008, *ApJ*, 684, L9
- Weinmann S. M., Kauffmann G., von der Linden A., De Lucia G., 2010, *MNRAS*, 406, 2249
- Weinmann S. M., van den Bosch F. C., Yang X., Mo H. J., 2006, *MNRAS*, 366, 2
- Wetzell A. R., Tinker J. L., Conroy C., 2012, *MNRAS*, 424, 232
- White S. D. M., Frenk C. S., 1991, *ApJ*, 379, 52
- Whitmore B. C., Gilmore D. M., Jones C., 1993, *ApJ*, 407, 489
- Yang X., Mo H. J., van den Bosch F. C., Pasquali A., Li C., Barden M., 2007, *ApJ*, 671, 153
- Yates R. M., Kauffmann G., 2014, *MNRAS*, 439, 3817
- Zhang W., Li C., Kauffmann G., Xiao T., 2013, *MNRAS*, 429, 2191
- Zwaan M. A., Meyer M. J., Staveley-Smith L., Webster R. L., 2005, *MNRAS*, 359, L30